Downloaded from orbit.dtu.dk on: May 20, 2025

DTU Library

# Effective surface conductivity of optical hyperbolic metasurfaces: from far-field characterization to surface wave analysis

**Yermakov, Oleh Y.; Permyakov, Dmitry V.; Porubaev, Filipp V.; Dmitriev, Pavel A.; Samusev, Anton K.; Iorsh, Ivan V.; Malureanu, Radu; Lavrinenko, Andrei V.; Bogdanov, Andrey A.**

*Published in:*
Scientific Reports

*Link to article, DOI:*
10.1038/s41598-018-32479-y

*Publication date:*
2018

*Document Version*
Publisher's PDF, also known as Version of record

Link back to DTU Orbit

*Citation (APA):*
Yermakov, O. Y., Permyakov, D. V., Porubaev, F. V., Dmitriev, P. A., Samusev, A. K., Iorsh, I. V., Malureanu, R., Lavrinenko, A. V., & Bogdanov, A. A. (2018). Effective surface conductivity of optical hyperbolic metasurfaces: from far-field characterization to surface wave analysis. *Scientific Reports*, *8*(1), Article 14135. https://doi.org/10.1038/s41598-018-32479-y

**General rights**
Copyright and moral rights for the publications made accessible in the public portal are retained by the authors and/or other copyright owners and it is a condition of accessing publications that users recognise and abide by the legal requirements associated with these rights.

- Users may download and print one copy of any publication from the public portal for the purpose of private study or research.
- You may not further distribute the material or use it for any profit-making activity or commercial gain
- You may freely distribute the URL identifying the publication in the public portal

If you believe that this document breaches copyright please contact us providing details, and we will remove access to the work immediately and investigate your claim.

SCIENTIFIC REPORTS

OPEN

# Effective surface conductivity of optical hyperbolic metasurfaces: from far-field characterization to surface wave analysis

Received: 12 April 2018
Accepted: 3 September 2018
Published online: 20 September 2018

Oleh Y. Yermakov[1], Dmitry V. Permyakov[1], Filipp V. Porubaev[2], Pavel A. Dmitriev[1], Anton K. Samusev[1], Ivan V. Iorsh[1], Radu Malureanu[3], Andrei V. Lavrinenko[1,3] & Andrey A. Bogdanov[1]

**Metasurfaces offer great potential to control near- and far-fields through engineering optical properties of elementary cells or meta-atoms. Such perspective opens a route to efficient manipulation of the optical signals both at nanoscale and in photonics applications. In this paper we show that a local surface conductivity tensor well describes optical properties of a resonant plasmonic hyperbolic metasurface both in the far-field and in the near-field regimes, where spatial dispersion usually plays a crucial role. We retrieve the effective surface conductivity tensor from the comparative analysis of experimental and numerical reflectance spectra of a metasurface composed of elliptical gold nanoparticles. Afterwards, the restored conductivities are validated by semi-analytic parameters obtained with the nonlocal discrete dipole model with and without interaction contribution between meta-atoms. The effective parameters are further used for the dispersion analysis of surface plasmons localized at the metasurface. The obtained effective conductivity describes correctly the dispersion law of both quasi-TE and quasi-TM plasmons in a wide range of optical frequencies as well as the peculiarities of their propagation regimes, in particular, topological transition from the elliptical to hyperbolic regime with eligible accuracy. The analysis in question offers a simple practical way to describe properties of metasurfaces including ones in the near-field zone with effective conductivity tensor extracting from the convenient far-field characterization.**

Miniaturization of integrated optical circuits requires an effective control of light on the subwavelength scale. Significant advances in this field have been achieved with the help of metamaterials[1–3] – artificially created media, whose electromagnetic properties can drastically differ from the properties of the natural materials. However, a three-dimensional structure of metamaterials, related fabrication challenges and high costs, especially for optical applications, form significant obstacles for their implementation in integrated optical circuits.

An alternative way is to use *metasurfaces* – two-dimensional analogues of metamaterials. There are also natural two-dimensional anisotropic materials such as hexagonal boron nitride[4,5], transition metal dichalcogenides[6,7], black phosphorus[8]. In the visible and the near-IR range, metasurfaces can be implemented using subwavelength periodic arrays of plasmonic or high-index dielectric nanoparticles[9–12]. A nanostructured graphene could also be considered as a metasurface for THz frequencies[13,14]. In the microwave range, metasurfaces can be implemented by using LC-circuits, split-ring resonators, arrays of capacitive and inductive elements (strips, grids, mushrooms), wire medium etc[15,16]. Despite subwavelength or even monoatomic thicknesses, the metasurfaces offer unprecedented control over light propagation, reflection and refraction[15,17].

Metasurfaces exhibit a lot of intriguing properties for a wide area of applications such as near-field microscopy, imaging, holography, biosensing, photovoltaics etc.[10,15–19]. For instance, it was shown that metasurfaces based on Si nanoparticles can exhibit nearly 100% reflectance[20] and transmittance[21] in a broadband frequency

[1]Department of Nanophotonics and Metamaterials, ITMO University, St. Petersburg, 197101, Russia. [2]Department of Biblical Studies, St. Petersburg Theological Academy, St. Petersburg, 191167, Russia. [3]DTU Fotonik, Technical University of Denmark, Oersteds pl. 343, DK-2800, Kongens Lyngby, Denmark. Correspondence and requests for materials should be addressed to O.Y.Y. (email: o.yermakov@metalab.ifmo.ru)

range. Moreover, metasurfaces can serve as light control elements: frequency selectors, antennas, lenses, perfect absorbers[16]. They offer an excellent functionality with polarization conversion, beam shaping and optical vortices generation[22,23]. Besides, metasurfaces provide an efficient control over dispersion and polarization of surface waves[24–30]. Surface plasmon-polaritons propagating along a metasurface assist pushing, pulling and lateral optical forces in its vicinity[31,32]. Metasurfaces are prospective tools for spin-controlled optical phenomena[33–36] and holographic applications[37–39]. Particular attention is paid to hyperbolic metasurfaces, which are promising tools for many applications including the manipulation over surface waves[26,40–42]. The main advantages of metasurfaces, such as relative manufacturing simplicity, rich functionality and planar geometry, fully compatible with modern fabrication technologies, create a promising platform for the *photonic metadevices*. It has been recently pointed out that all-dielectric metasurfaces and metamaterials can serve as a prospective low-loss platform, which could replace plasmonic structures[43]. However, one of the main advantages of plasmonic structures, unachievable with dielectric ones, is that the plasmonic structures can be resonant in the visible range keeping at the same time a deep subwavelength thickness and period. Thus, here we concentrate on plasmonic metasurfaces allowing light manipulation with a deep subwavelength structure.

The common feature of bulk metamaterials and metasurfaces is that due to the subwavelength structure they can be considered as homogenized media described by effective material parameters. For bulk metamaterials, such effective parameters are permittivity $\hat{\varepsilon}_{\text{eff}}$ and/or permeability $\hat{\mu}_{\text{eff}}$. Retrieving effective parameters is one of the most important problems in the study of metamaterials. Generally, the effective parameters are tensorial functions of frequency $\omega$, wavevector $\mathbf{k}$, and intensity $I$. Homogenization of micro- and nanostructured metamaterials can become rather cumbersome, especially taking into account nonlocality[44–46], chirality[47], bi-anisotropy[48,49] and nonlinearity[50,51].

Analogous homogenization procedures are relevant for metasurfaces. Apparently, homogenization procedures for 2D structures were firstly developed in radiophysics and microwaves (equivalent surface impedance) in applications to thin films, high-impedance surfaces and wire grids etc[52–54]. It has been recently pointed out that two-dimensional structures, like graphene, silicene and metasurfaces, can be described within an effective conductivity approach[24,25,55–58]. In virtue of a subwavelength thickness, a metasurface could be considered as a two-dimensional equivalent current and, therefore, characterized by effective electric $\hat{\sigma}_e(\omega, \mathbf{k}_\tau)$ and magnetic $\hat{\sigma}_m(\omega, \mathbf{k}_\tau)$ surface conductivity tensors, where $\mathbf{k}_\tau$ is the component of the wavevector in the plane of the metasurface[15,16]. Importantly, such effective surface conductivity describes the properties of the metasurface both in the far-field when $|\mathbf{k}_\tau| < \omega/c$ (reflection, absorption, refraction, polarization transformation etc.) and in the near-field (surface waves, Purcell effect, optical forces), when $|\mathbf{k}_\tau| > \omega/c$.

In this paper, we focus our study on a resonant plasmonic anisotropic metasurface represented by a two-dimensional periodic array of gold nanodisks with the elliptical base. We derive and analyze the electric surface conductivity tensor of the anisotropic metasurface in three ways: (i) numerically by combining the optical measurements of the fabricated metasurface, simulations of the experiment and analytical approach (zero-thickness approximation); (ii) experimentally by characterization of the metasurface reflection spectra and a subsequent fitting with Drude-Lorentz formula; and (iii) theoretically by using the nonlocal discrete dipole model. We reveal that the effective surface conductivity tensor extracted from the far-field measurements well describes near-field properties of metasurface such as the spectrum of surface waves and their behaviour in all possible regimes - capacitive, inductive, and hyperbolic. By using the discrete dipole model we study the effects of spatial dispersion on the eigenmodes spectrum and define the limitations of the effective model applicability.

## Sample Design and Fabrication

We consider a metasurface composed of gold anisotropic nanoparticles placed on a fused silica substrate. The design of the sample is shown in Fig. 1. The target structure consists of 20 nm thick gold nanodisks with the elliptical base packed in the square lattice with a period of 200 nm. The average long and short axes of the disks are $a_x = 134$ nm and $a_y = 103$ nm, respectively. The distribution of the nanodisks sizes is provided in Fig. S1 (See Supplementary Information S1).

The sample was fabricated via electron beam lithography on a fused silica substrate. Before the electron beam exposure process, the resist layer (PMMA) was covered with a thin gold layer to prevent local charge accumulation. After the exposure, a 20 nm thick gold layer was sputtered via thermal evaporation. During the last step of the fabrication process, the remains of the resist were removed via the lift-off procedure. Finally, the sample was immersed in a liquid with a refractive index nearly matching the glass substrate. Thus, we obtained the metasurface with a homogeneous ambient medium with permittivity $\varepsilon = 2.1$. The SEM image of the fabricated sample is shown in Fig. 1a.

## Effective Conductivity Tensor

The plasmonic resonant metasurface shown in Fig. 1 is anisotropic and non-chiral. Asymmetry of each particle splits its in-plane dipole plasmonic resonance with frequency $\Omega$ into two resonances with frequencies $\Omega_\perp$ and $\Omega_\parallel$[24,29]. Consideration of metasurfaces as an absolutely flat object might be restricted due to the emergence of the out-of-plane polarizability caused by the finite thickness of the plasmonic particles. In our case, the out-of-plane polarizability $\alpha_z$ could be neglected due to a small thickness of the particles as it is shown in Fig. S2 (See Supplementary Information S2). Therefore, this metasurface can be described by a two-dimensional effective surface conductivity tensor, which is diagonal in the principal axes (when the axes of the coordinates system are parallel to the axes of the elliptical base of the nanodisks).

**Numerical vs Experimental Characterization.** To extract the effective surface conductivity of the fabricated sample, we apply a procedure based on the combination of the optical experiments, numerical simulations and theoretical calculations.

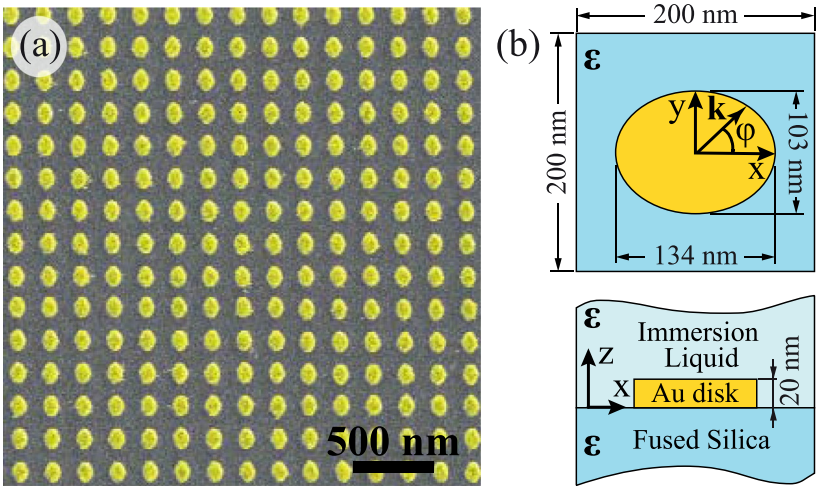


**Figure 1.** (**a**) False color SEM image of the fabricated anisotropic metasurface. (**b**) The structure consists of 20-nm-thick gold nanodisks arranged in a square lattice (period 200 nm). The base of the disks has an elliptical shape, with the long and short axes equal to 134 and 103 nm, respectively. We assume the environment is uniform and isotropic with $\varepsilon = 2.1$.

First, we measure the intensity of the reflectance for the light polarized along and across the principle axes of the metasurface under normal incidence (Fig. 2a). Both spectra demonstrate single peaks corresponding to the individual localized plasmon resonances of the nanodisks. The phase retrieved by the fitting of the experimental reflectance with the intensity calculated by the use of the Drude formula (See Supplementary Information S3) is shown in Fig. 2a by the red lines.

Then, we model the experiment with CST Microwave Studio (Fig. 2b). The difference in the intensity of the peaks in Fig. 2a,b can be attributed to roughness and inhomogeneity of the sample. We obtain similar values of reflectance spectra from the experiment and simulation by increasing the imaginary part of the gold permittivity in the simulation (See Supplementary Information S3). The minor shift of the resonance position can be associated with a small difference between the immersion liquid and fused silica substrate permittivities (See Supplementary Information S7). In order to retrieve a complex conductivity tensor we take the intensity and the phase of reflection coefficient from the simulation, wherein we obtain good matching between the simulated and experimental shapes of the reflectance spectra (Fig. 2a,b).

Basing on the calculated complex reflection coefficient we find an effective surface conductivity using the zero-thickness approximation (ZTA). Within this approximation we replace the real structure of finite thickness $H$ by the effective two-dimensional plane disposed at distance $H/2$ from the substrate. This technique can be applied only for deeply subwavelength structures. The limitation can be formulated as $H/\lambda \ll 1$ according to the Nicolson-Ross-Weir method[59,60].

Considering a two-dimensional layer with effective conductivity $\sigma$ sandwiched between two media with refractive indices $n_1$ (superstrate) and $n_2$ (substrate) one can find Fresnel's coefficients[55,61,62] and express the effective surface conductivity as follows

$$\sigma_{x,y} = \frac{n_1 - n_2 - S_{11}^{x,y}(n_1 + n_2)}{1 + S_{11}^{x,y}}, \tag{1}$$

where $S_{11}^{x,y}$ is the component of the $S$-matrix. Indices $x$, $y$ correspond to different orientations of the electric field of the incident wave. Hereinafter we use the Gauss system of units and express surface conductivity in the dimensionless units $\sigma = 4\pi\tilde{\sigma}/c$. The proposed extraction technique may be applied even in the case of the arbitrary incident angle (See Supplementary Information S4). In this case, one can obtain the dependence of the retrieved conductivity on the in-plane wavevector, which allows to define the impact of spatial dispersion.

In order to obtain the proper conductivity of a metasurface one should retain only the phase of the reflection coefficient related to the metasurface properties. In the simulation, the total phase of the $S$-parameters has two contributions $\arg(S_{11}^{x,y}) = \Delta\varphi_1 + \Delta\varphi_2$. The first one arises directly when the wave reflects from the metasurface. The second phase arises because of the wave propagation from the port to the metasurface and back $\Delta\varphi_2 = 2k_0L$. Here, the time dependence is defined through the factor $e^{i\omega t}$, $k_0 = n_1\omega/c$, $L$ is the distance between the excitation port and the metasurface. The problem is how to correctly determine distance $L$ if the metasurface has a finite thickness? We found that the correct results not breaking the energy conservation law (See Supplementary Information S5) are obtained only if $L$ is defined as the distance to the middle of the metasurface. Thus, the effective two-dimensional layer has to be disposed exactly at distance $H/2$ from the substrate. The obvious analogue of ZTA is the transfer matrix method (TMM), which originates from Fresnel's reflection and transmission coefficients. For the metasurface under consideration ZTA and TMM give the results with the average relative error of 1%. However, the advantage of ZTA over TMM is that it is necessary to know only one either reflection or transmission coefficient to extract the effective parameters. The effective conductivity retrieved from the far-field

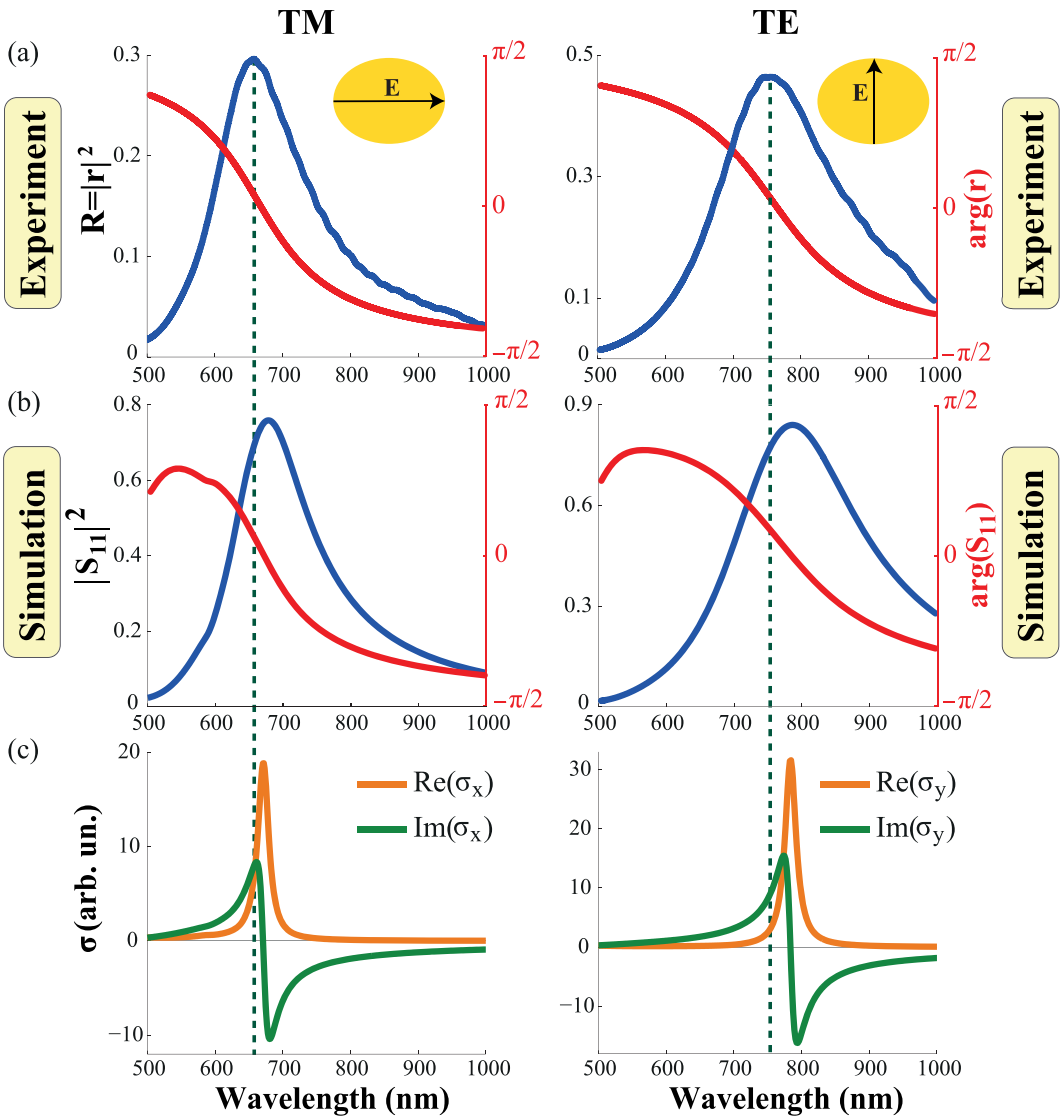


**Figure 2.** Reflectance spectra of a metasurface for polarization along (left panel) and across (right panel) the long axis of the disk. (**a**) Intensity (blue lines) and phase (red lines) of the reflectance spectra obtained from the experimental measurements. (**b**) Squared moduli (blue lines) and phases (red lines) of the metasurface reflection coefficient $S_{11}$ calculated in CST Microwave Studio. (**c**) Real (orange lines) and imaginary (green lines) parts of the TM- and TE-polarized components of the effective surface conductivity tensor extracted from $S_{11}$ data via ZTA.

measurements correctly predicts the near-field properties. In particular, it describes well the surface waves spectrum. It is possible due to the non-critical contribution of the spatial dispersion.

The extracted conductivities for both polarizations are presented in Fig. 2c. For the light wave polarized along the long axis (TM-polarization) the plasmon resonance is observed at 670 nm, while for light polarized along the short axis (TE-polarization) the resonance corresponds to 780 nm.

**Discrete Dipole Model.** In order to derive surface conductivity of a metasurface analytically we apply the *discrete dipole model* (DDM), in many works it is also called the *point-dipole model*. This technique has been implemented for 1D, 2D and 3D structures[63–67]. Within this approach we consider a 2D periodic array of the identical scatterers as an array of point dipoles.

In the framework of the DDM it is more convenient to operate with an effective polarizability of the structure, which is straightforwardly connected to the effective conductivity tensor as follows:

$$\hat{\sigma}_{\text{eff}} = -i\frac{4\pi\varepsilon\omega}{ca^2}\hat{\alpha}_{\text{eff}}. \tag{2}$$

In the case under consideration, the thickness of the scatterers is deeply subwavelength and, therefore, we can neglect the polarizability of the particles in the direction perpendicular to the plane of the metasurface. Thus, we

can describe the metasurface by either two-dimensional polarizability tensor $\hat{\alpha}_{\text{eff}}$ or conductivity tensor $\hat{\sigma}_{\text{eff}}$ with zero off-diagonal components (in the basis of the principal axes). Rigorous derivation of the effective polarizability of a two-dimensional lattice of resonant scatterers is performed in Refs.[49,65,68]. The effective polarizability of the metasurface can be written as

$$\hat{\alpha}_{\text{eff}}^{-1}(\omega, \mathbf{k}_{\tau}) = \hat{\alpha}_0^{-1}(\omega) + \hat{C}(\omega, \mathbf{k}_{\tau}). \tag{3}$$

Here, $\hat{\alpha}_0(\omega)$ is the polarizability of the individual resonant scatterer, and $\hat{C}(\omega, \mathbf{k}_{\tau})$ is the so-called dynamic interaction constant[65]. The latter contains the *lattice sum*, which takes into account interaction of each dipole with all others. We approximate the polarizability of the disk with the elliptical base $\hat{\alpha}_0$ by the polarizability of an ellipsoid with the same volume and aspect ratio (See Supplementary Information S2). We calculate the interaction between the identical scatterers by using the Green's function formalism:

$$\hat{C}(\omega, \mathbf{k}_{\tau}) = \sum_{i,j} \hat{G}(\omega, \mathbf{r}_{ij}) e^{i\mathbf{k}_{\tau}\mathbf{r}_{ij}}. \tag{4}$$

Here $\hat{G}(\omega, \mathbf{r}_{ij})$ is the dyadic Green's function and $\mathbf{r}_{ij}$ are the coordinates of the dipoles. This sum has slow convergence. So, we calculate the interaction term in Eq. (4) within the Ewald summation technique[63,66,69,70] applied for a two-dimensional periodic structure, which ensures fast convergence of the sum (See Supplementary Information S6).

The discrete dipole model can be successfully applied for many types of metasurfaces. It is applicable for two-dimensional periodic structures under three main conditions:

1. Quasistatic condition: $na \ll \lambda$. Here $n$ is the refractive index of the environment, $a$ is the lattice constant, $\lambda$ is the incident wavelength.
2. Dipole approximation: $f \ll 1$ (or $d \ll a$, where $d$ is the characteristic size of a scaterrer). Here $f = A/a^2$ is the filling factor, $A$ is the area occupied by the scatterer in the unit cell (in our case, $A = \pi a_x a_y$), $a^2$ is the area of the square unit cell. When the scatterers are not sufficiently small one has to take into account higher order multipoles.
3. Quasi-two-dimensionality: $a_{zz} \ll \min(a_{xx}, a_{yy})$ and $H \ll \lambda$. This condition is achieved, when thickness of a metasurface is less than both characteristic in-plane sizes of meta-atoms ($H < \min\{a_x, a_y\}$) and skin depth $\delta$ ($H < \delta$).

For the metasurface sample under consideration $H/a_y = 0.19$, and $f = 0.27$. Although the applicability condition of the dipole approximation is poorly satisfied, the DDM gives eligible results. Parameters $na/\lambda$ and $H/\lambda$ lie in the interval from 0.25 to 0.75 and from 0.02 to 0.05, respectively, for wavelengths $\lambda = 400$–$1200$ nm. Skin depth $\delta$ for gold is around 20–40 nm in the wavelength range under consideration[71].

One can see in Fig. 3a,c that neglecting interaction term $\hat{C}(\omega, \mathbf{k}_{\tau})$ in Eq. (3) results in a blue shift of the conductivity spectra by several tens of nanometers for both polarizations. Accounting these interactions brings the DDM into almost perfect agreement with the ZTA (Fig. 3b,d). However, matching for $\sigma_y$ is better than for $\sigma_x$. It could be explained by the fact that polarizability of an ellipsoid approximates polarizability of the elliptical disk in the $y$ direction better that in the $x$ direction.

The spectral dependences of the extracted surface conductivities along the principal axes are shown in Figs. 2c and 3. They clearly show that the fabricated metasurface is characterized by a highly anisotropic resonant conductivity tensor:

$$\hat{\sigma}_{\text{eff}} = \begin{pmatrix} \sigma_x & 0 \\ 0 & \sigma_y \end{pmatrix}. \tag{5}$$

One can see from Fig. 2c that the metasurface supports three different regimes depending on wavelength $\lambda$ of the incident light. These regimes can be classified by the signs of (i) $\det[\text{Im}(\hat{\sigma})]$ and (ii) $\text{tr}[\text{Im}(\hat{\sigma})]$. Specifically, when $\det[\text{Im}(\hat{\sigma})] > 0$ and $\text{tr}[\text{Im}(\hat{\sigma})] > 0$ (for $\lambda < 670$ nm) the inductive regime of the metasurface is observed. In this case, the metasurface corresponds to the conventional metal sheet and only a TM-polarized surface wave can propagate. For $\det[\text{Im}(\hat{\sigma})] > 0$ and $\text{tr}[\text{Im}(\hat{\sigma})] < 0$ (for $\lambda > 780$ nm) the capacitive regime of the metasurface is met, so only a TE-polarized surface wave can propagate. When $\det[\text{Im}(\hat{\sigma})] < 0$ (between the resonances, i.e. for wavelengths from 670 to 780 nm), a metasurface supports the so-called *hyperbolic* regime, in which simultaneous propagation of both TE- and TM-modes is possible[24].

## Surface Waves

The dispersion equation of the surface waves supported by an anisotropic metasurface, described by the effective conductivity tensor (5), can be straightforwardly derived from Maxwell's equations and boundary conditions at the metasurface[24]:

$$\left(\frac{c\kappa_1}{\mu_1\omega} + \frac{c\kappa_2}{\mu_2\omega} - i\sigma_{xx}\right)\left(\frac{\varepsilon_1\omega}{c\kappa_1} + \frac{\varepsilon_2\omega}{c\kappa_2} + i\sigma_{yy}\right) = \sigma_{xy}\sigma_{yx}. \tag{6}$$

Here, $\sigma_{ij}$ are the tensor components in the coordinate system rotated by angle $\varphi$ (see Fig. 1b), $\varepsilon_1$, $\mu_1$, $\kappa_1$ and $\varepsilon_2$, $\mu_2$, $\kappa_2$ are the permittivity, permeability and inverse penetration depths of the wave in the superstrate and substrate,

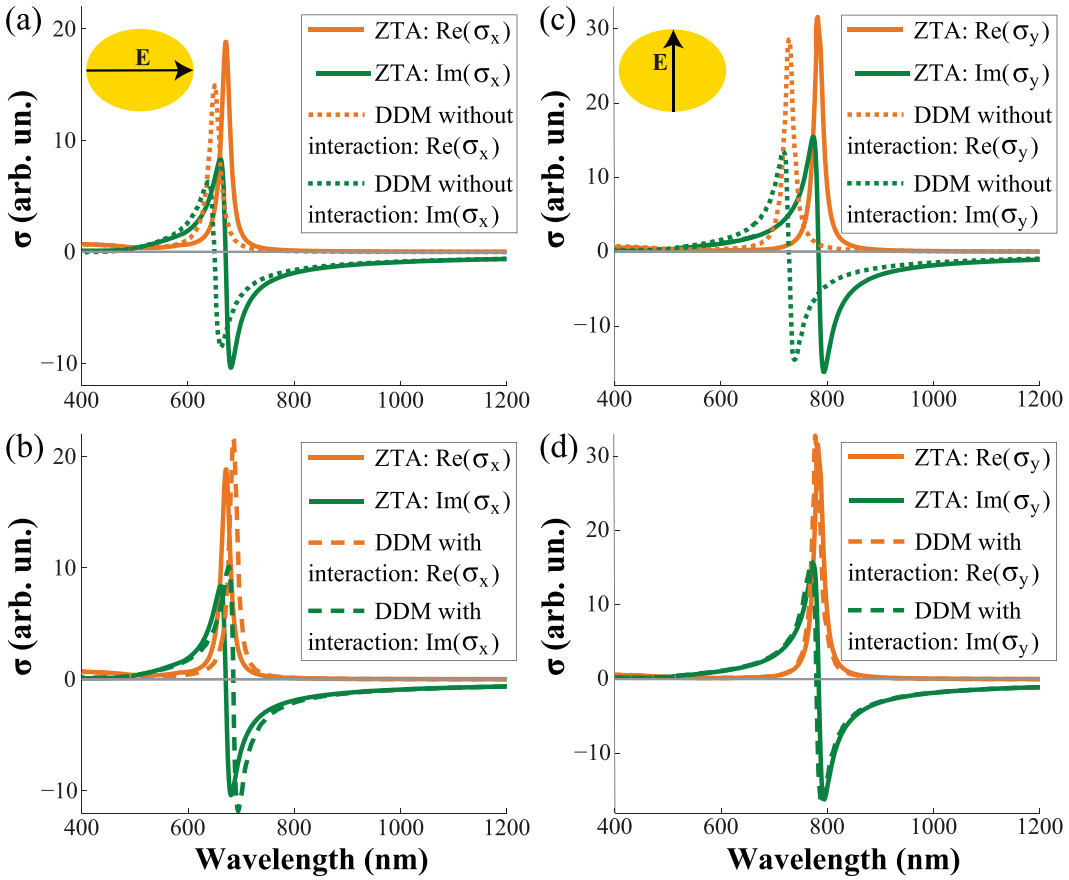


**Figure 3.** Real (orange lines) and imaginary (green lines) parts of the effective conductivity extracted via ZTA (solid lines), DDM without interaction (dotted lines) and DDM with interaction (dashed lines) for TM (**a**,**b**) and TE (**c**,**d**) polarizations.

respectively. The latter is defined as $\kappa_i = \sqrt{\mathbf{k}_\tau^2 - \varepsilon_i \mu_i \omega^2/c^2}$, where $\mathbf{k}_\tau$ is the wavevector in the plane of the metasurface. In our case Eq. (6) is simplified since we consider the metasurface in non-magnetic ($\mu_1 = \mu_2 = 1$) and homogeneous environment with the permittivity corresponding to fused silica $\varepsilon = \varepsilon_1 = \varepsilon_2 = 2.1$.

The first and the second factors in the left side of Eq. (6) correspond to the dispersion of purely TE-polarized and TM-polarized surface waves, respectively. The right side of Eq. (6) is the coupling factor responsible for the mixing of TE and TM modes. If an electromagnetic wave propagates along a principal axis the coupling factor is zero, so either a conventional TM-plasmon or TE-plasmon exists. However, due to anisotropy ($\varphi \neq 0°$) the coupling factor can become non-zero giving rise to hybrid surface waves of mixed TE-TM polarizations. Despite the hybridization, only one type of polarization is predominant for each mode. Therefore, it is logical to refer to such modes as *quasi-TM* and *quasi-TE* surface plasmons.

It is important to note that for a number of practical problems it is necessary to take into account nonlocal effects caused by spatial dispersion. For instance, it was shown that the intrinsic graphene nonlocality may have a significant impact on the properties of surface plasmons propagating along the hyperbolic metasurface based on the graphene strips[72]. Unfortunately, it can not be accounted for in the framework of the effective surface conductivity extracted from the normal incidence measurements. However, it can be calculated by using lattice sums. In this case, the dispersion equation for the eigenmodes has the following form:

$$\det|\hat{\alpha}_{\text{eff}}^{-1}(\omega, \mathbf{k}_\tau)| = \det|\hat{\alpha}_0^{-1}(\omega) + \hat{C}(\omega, \mathbf{k}_\tau)| = 0. \tag{7}$$

Equation (7) can be transformed into Eq. (6) under the assumption that $d \ll a \ll \lambda$.

Figure 4 shows the dispersion of the surface waves localized at the studied metasurface sample for different propagation angles $\varphi = 0, 45, 90°$. In Figs. 4a–c we compare the effective model and the discrete dipole model taking into account spatial dispersion ($\mathbf{k}_\tau \neq \mathbf{0}$). One can see that the difference in the dispersions obtained within the local and nonlocal models is significant. It can be explained by quite a large filling factor *f*, which sharply limits the accounting for nonlocal effects in the framework of the discrete dipole model. Nevertheless, both models are qualitatively similar. For instance, the resonant frequencies are close in both models for all propagation angles. Both models predict the frequency gap between TM- and TE-plasmons for $\varphi = 0°$ which shrinks with increasing of $\varphi$. At $\varphi = 90°$, the gap disappears and both surface modes can propagate at the same frequency, that is in accordance with the results of full-wave numerical simulations (see Fig. 4f). Better matching between the

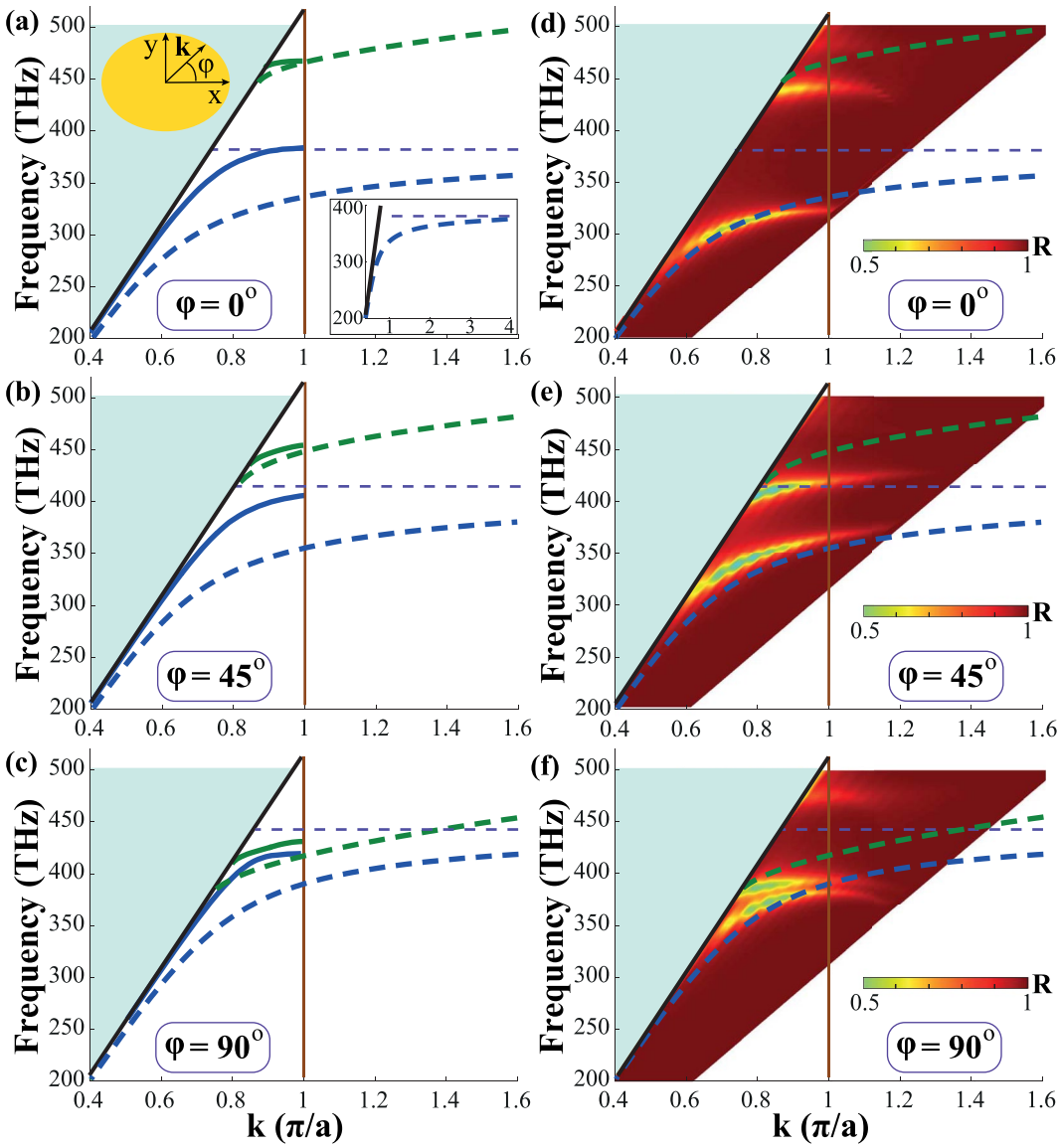


**Figure 4.** Dispersion of the quasi-TE (blue lines) and the quasi-TM (green lines) surface plasmons for different propagation angles (**a**,**d**) $\varphi = 0°$, (**b**,**e**) $\varphi = 45°$, (**c**,**f**) $\varphi = 90°$. Dashed lines correspond to the dispersion calculated within the effective conductivity approximation. Solid lines correspond to the calculations taking into account nonlocal interactions via the lattice sums (**a**–**c**). Color map shows the reflectance spectra of the metasurface coupled to a high-index prism with the mixed TE-TM polarization (**d**–**f**). The light line in the medium with permittivity $\varepsilon = 2.1$ is shown as the black line. The boundary of the first Brillouin zone is shown as the vertical solid line. The horizontal purple dashed line corresponds to the plasmon resonance according to the effective model as the insert in sub-picture (**a**) shows.

results of DDM and full-wave simulations could be obtained if we account for anisotropy of the dynamic interaction constant, but this theoretical extension is the subject of our further research.

To check the applicability of the effective conductivities extracted from the far-field measurements in characterization of the near-field phenomena, we compare dispersion of the surface waves from Figs. 4a-c with the results from full-wave numerical simulations carried out in COMSOL Multiphysics (Figs. 4d–f). One can see good correspondence of bands at low frequencies (for the quasi-TE mode). At high frequencies, i.e. small wavelengths, the effective model works worse but it is still eligible for qualitative results.

It is convenient to present dispersion of surface waves in terms of equal frequency contours, which can be visualized in reflection experiments with a high index ZnSe prism in Otto geometry. We calculate reflection of a light wave in such a configuration by using the transfer matrix method[73]. When $\det[\mathrm{Im}(\hat{\sigma})] > 0$, the equal frequency contours have an elliptic shape (Fig. 5a,c,d,f). For a hyperbolic regime, when $\det[\mathrm{Im}(\hat{\sigma})] < 0$ ($\lambda = 730$ nm), the equal frequency contours represent a set of hyperbolas for the quasi-TE mode (Fig. 5b) and arcs for the quasi-TM mode (Fig. 5e). This drastic change of the shape is often called *topological transition*. One can see that in the hyperbolic regime both quasi-TE and quasi-TM modes are present, i.e. simultaneous propagation of two

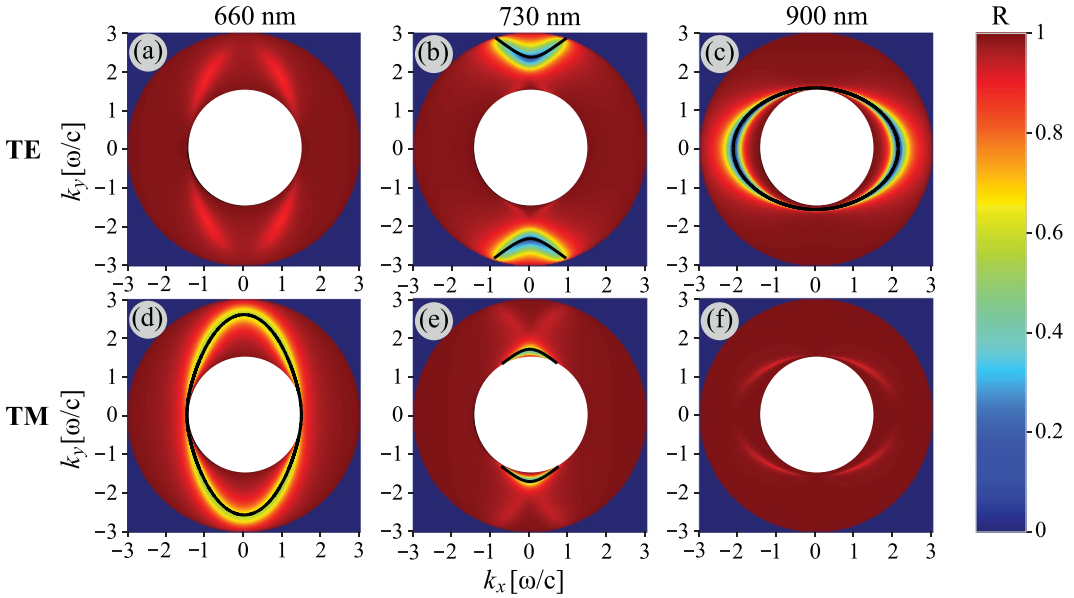


**Figure 5.** Simulation of the reflectance spectra from a metasurface shown in Fig. 1 for incident TE (**a**–**c**) and TM (**d-f**) polarizations. Panels (a) and (d), (b) and (e), (c) and (f) correspond to wavelengths $\lambda = 660$, 730, 900 nm, respectively. Black lines correspond to the equal frequency contours calculated from Eq. (6) straightforwardly. White circles correspond to the light cone with $n = 1.45$, while big circles correspond to the light line in ZnSe with $n = 2.48$.

types of surface plasmons is observed (Fig. 5b,e), which is consistent with bands dispersion in Fig. 4c,f. For the capacitive and inductive regimes only a single mode propagates. However, each mode has hybrid TE-TM polarization, so it is observed in both polarizations as shown in Fig. 5. Although polarization of the surface mode at 660 nm is predominantly similar to polarization of a conventional TM-plasmon (Fig. 5d), TE-polarization is also visible (Fig. 5a). The opposite situation takes place for a quasi-TE plasmon at $\lambda = 900$ nm (Fig. 5c,f). The exceptions are the principal axes directions where polarization of surface modes is strictly either purely TE or purely TM due to the lack of anisotropy.

## Conclusions

To conclude, we have suggested a practical concept to describe the full set of optical properties of a metasurface. Our approach is based on extraction of the effective surface conductivity. It allows to study various phenomena in the far-field as well as to calculate the spectrum of surface waves. We have developed two techniques to retrieve the effective conductivity and discussed their limitations. There are three different regimes of the local diagonal conductivity tensor of the anisotropic metasurface composed of elliptical gold nanodisks: inductive (metal-like), capacitive (dielectric-like) and hyperbolic (like in an indefinite medium). In contrast to an isotropic metasurface such anisotropic metasurface supports two modes of hybrid polarizations. We have shown the influence of non-locality on dispersion of the surface waves. Finally, we have demonstrated the topological transition of the equal frequency contours and the hybridization of two eigenmodes in the optical and mid-IR ranges. We believe these results will be highly useful for a plethora of metasurfaces applications in nanophotonics, plasmonics, sensing and opto-electronics.

## References

1. Smith, D. R., Pendry, J. B. & Wiltshire, M. C. Metamaterials and negative refractive index. *Science* **305**, 788–792 (2004).
2. Engheta, N. & Ziolkowski, R. W. Metamaterials: physics and engineering explorations (John Wiley & Sons, 2006).
3. Shalaev, V. M. Optical negative-index metamaterials. *Nat. Photonics* **1**, 41–48 (2007).
4. Dai, S. *et al*. Subdiffractional focusing and guiding of polaritonic rays in a natural hyperbolic material. *Nat. Commun.* **6**, 6963 (2015).
5. Li, P. *et al*. Hyperbolic phonon-polaritons in boron nitride for near-field optical imaging. *Nat. Commun.* **6**, 7507 (2015).
6. Hamm, J. M. & Hess, O. Two two-dimensional materials are better than one. *Science* **340**, 1298–1299 (2013).
7. Glazov, M. *et al*. Exciton fine structure and spin decoherence in monolayers of transition metal dichalcogenides. *Phys. Rev. B* **89**, 201302 (2014).
8. Correas-Serrano, D., Gomez-Diaz, J., Melcon, A. A. & Alù, A. Black phosphorus plasmonics: anisotropic elliptical propagation and nonlocality-induced canalization. *J. Opt.* **18**, 104006 (2016).
9. Kildishev, A. V., Boltasseva, A. & Shalaev, V. M. Planar photonics with metasurfaces. *Science* **339**, 1232009 (2013).
10. Yu, N. & Capasso, F. Flat optics with designer metasurfaces. *Nat. Mater.* **13**, 139 (2014).
11. Meinzer, N., Barnes, W. L. & Hooper, I. R. Plasmonic meta-atoms and metasurfaces. *Nat. Photonics* **8**, 889–898 (2014).
12. Kuznetsov, A. I., Miroshnichenko, A. E., Brongersma, M. L., Kivshar, Y. S. & Luk'yanchuk, B. Optically resonant dielectric nanostructures. *Science* **354**, aag2472 (2016).
13. Christensen, J., Manjavacas, A., Thongrattanasiri, S., Koppens, F. H. & Garcia de Abajo, F. J. Graphene plasmon waveguiding and hybridization in individual and paired nanoribbons. *ACS Nano* **6**, 431–440 (2011).
14. Trushkov, I. & Iorsh, I. Two-dimensional hyperbolic medium for electrons and photons based on the array of tunnel-coupled graphene nanoribbons. *Phys. Rev. B* **92**, 045305 (2015).

15. Holloway, C. L. *et al*. An overview of the theory and applications of metasurfaces: The two-dimensional equivalents of metamaterials. *IEEE Antenn. Propag. M.* **54**, 10–35 (2012).
16. Glybovski, S. B., Tretyakov, S. A., Belov, P. A., Kivshar, Y. S. & Simovski, C. R. Metasurfaces: From microwaves to visible. *Phys. Rep.* **634**, 1–72 (2016).
17. Yu, N. & Capasso, F. Optical metasurfaces and prospect of their applications including fiber optics. *J. Lightwave Technol.* **33**, 2344–2358 (2015).
18. Chen, H.-T., Taylor, A. J. & Yu, N. A review of metasurfaces: physics and applications. *Rep. Prog. Phys.* **79**, 076401 (2016).
19. Ding, F., Pors, A. & Bozhevolnyi, S. I. Gradient metasurfaces: a review of fundamentals and applications. *Rep. Prog. Phys.* **81**, 026401 (2018).
20. Moitra, P., Slovick, B. A., Yu, Z. G., Krishnamurthy, S. & Valentine, J. Experimental demonstration of a broadband all-dielectric metamaterial perfect reflector. *Appl. Phys. Lett.* **104**, 171102 (2014).
21. Decker, M. *et al*. High-efficiency dielectric Huygens' surfaces. *Adv. Opt. Mater.* **3**, 813–820 (2015).
22. Yang, Y. *et al*. Dielectric meta-reflectarray for broadband linear polarization conversion and optical vortex generation. *Nano Lett.* **14**, 1394–1399 (2014).
23. Desiatov, B., Mazurski, N., Fainman, Y. & Levy, U. Polarization selective beam shaping using nanoscale dielectric metasurfaces. *Opt. Express* **23**, 22611–22618 (2015).
24. Yermakov, O. Y. *et al*. Hybrid waves localized at hyperbolic metasurfaces. *Phys. Rev. B* **91**, 235423 (2015).
25. Gomez-Diaz, J. S., Tymchenko, M. & Alù, A. Hyperbolic plasmons and topological transitions over uniaxial metasurfaces. *Phys. Rev. Lett.* **114**, 233901 (2015).
26. Gomez-Diaz, J. & Alù, A. Flatland optics with hyperbolic metasurfaces. *ACS Photonics* **3**, 2211–2224 (2016).
27. Takayama, O., Bogdanov, A. A. & Lavrinenko, A. V. Photonic surface waves on metamaterial interfaces. *J. Phys. Condens. Matter.* **29**, 463001 (2017).
28. Low, T. *et al*. Polaritons in layered two-dimensional materials. *Nat. Mater.* **16**, 182–194 (2017).
29. Samusev, A. *et al*. Polarization-resolved characterization of plasmon waves supported by an anisotropic metasurface. *Opt. Express* **25**, 32631–32639 (2017).
30. Ding, F., Deshpande, R. & Bozhevolnyi, S. I. Bifunctional gap-plasmon metasurfaces for visible light: polarization-controlled unidirectional surface plasmon excitation and beam steering at normal incidence. *Light Sci. Appl.* **7**, 17178 (2018).
31. Rodríguez-Fortuño, F. J., Engheta, N., Martnez, A. & Zayats, A. V. Lateral forces on circularly polarizable particles near a surface. *Nat. Commun.* **6**, 8799 (2015).
32. Petrov, M. I., Sukhov, S. V., Bogdanov, A. A., Shalin, A. S. & Dogariu, A. Surface plasmon polariton assisted optical pulling force. *Laser Photonics Rev.* **10**, 116–122 (2016).
33. Shitrit, N. *et al*. Spin-optical metamaterial route to spin-controlled photonics. *Science* **340**, 724–726 (2013).
34. Aiello, A., Banzer, P., Neugebauer, M. & Leuchs, G. From transverse angular momentum to photonic wheels. *Nat. Photonics* **9**, 789–795 (2015).
35. Bliokh, K. Y. & Nori, F. Transverse and longitudinal angular momenta of light. *Phys. Rep.* **592**, 1–38 (2015).
36. Yermakov, O. Y. *et al*. Spin control of light with hyperbolic metasurfaces. *Phys. Rev. B* **94**, 075446 (2016).
37. Huang, L. *et al*. Three-dimensional optical holography using a plasmonic metasurface. *Nat. Commun.* **4**, 2808 (2013).
38. Ni, X., Kildishev, A. V. & Shalaev, V. M. Metasurface holograms for visible light. *Nat. Commun.* **4**, 2807 (2013).
39. Zheng, G. *et al*. Metasurface holograms reaching 80% efficiency. *Nat. Nanotechnol.* **10**, 308–312 (2015).
40. Sedighy, S. H., Guclu, C., Campione, S., Amirhosseini, M. K. & Capolino, F. Wideband planar transmission line hyperbolic metamaterial for subwavelength focusing and resolution. *IEEE Transactions Antenn. Propag.* **61**, 4110–4117 (2013).
41. High, A. A. *et al*. Visible-frequency hyperbolic metasurface. *Nature* **522**, 192 (2015).
42. Li, P. *et al*. Infrared hyperbolic metasurface based on nanostructured van der Waals materials. *Science* **359**, 892–896 (2018).
43. Jahani, S. & Jacob, Z. All-dielectric metamaterials. *Nat. Nanotechnol.* **11**, 23–36 (2016).
44. Simovski, C. R. On electromagnetic characterization and homogenization of nanostructured metamaterials. *J. Opt.* **13**, 013001 (2010).
45. Pors, A., Tsukerman, I. & Bozhevolnyi, S. I. Effective constitutive parameters of plasmonic metamaterials: homogenization by dual field interpolation. *Phys. Rev. E* **84**, 016609 (2011).
46. Chebykin, A., Orlov, A., Simovski, C., Kivshar, Y. S. & Belov, P. A. Nonlocal effective parameters of multilayered metal-dielectric metamaterials. *Phys. Rev. B* **86**, 115420 (2012).
47. Andryieuski, A. *et al*. Homogenization of resonant chiral metamaterials. *Phys. Rev. B* **82**, 235107 (2010).
48. Ouchetto, O., Qiu, C.-W., Zouhdi, S., Li, L.-W. & Razek, A. Homogenization of 3-D periodic bianisotropic metamaterials. *IEEE T. Microw. Theory* **54**, 3893–3898 (2006).
49. Alù, A. First-principles homogenization theory for periodic metamaterials. *Phys. Rev. B* **84**, 075153 (2011).
50. Mackay, T. G. Linear and nonlinear homogenized composite mediums as metamaterials. *Electromagn.* **25**, 461–481 (2005).
51. Larouche, S. & Smith, D. R. A retrieval method for nonlinear metamaterials. *Opt. Commun.* **283**, 1621–1627 (2010).
52. MacFarlane, G. Surface impedance of an infinite parallel-wire grid at oblique angles of incidence. *J. Inst. Electr. Eng. Part IIIA: Radiolocation* **93**, 1523–1527 (1946).
53. Klein, N. *et al*. The effective microwave surface impedance of high T thin films. *J. Appl. Phys.* **67**, 6940–6945 (1990).
54. Tretyakov, S. & Maslovski, S. Thin absorbing structure for all incidence angles based on the use of a highimpedance surface. *Microw. Opt. Techn. Lett.* **38**, 175–178 (2003).
55. Andryieuski, A. & Lavrinenko, A. V. Graphene metamaterials based tunable terahertz absorber: effective surface conductivity approach. *Opt. Express* **21**, 9144–9155 (2013).
56. Tabert, C. J. & Nicol, E. J. Magneto-optical conductivity of silicene and other buckled honeycomb lattices. *Phys. Rev. B* **88**, 085434 (2013).
57. Danaeifar, M., Granpayeh, N., Mortensen, N. A. & Xiao, S. Equivalent conductivity method: straightforward analytical solution for metasurface-based structures. *J. Phys. D Appl. Phys.* **48**, 385106 (2015).
58. Nemilentsau, A., Low, T. & Hanson, G. Anisotropic 2D materials for tunable hyperbolic plasmonics. *Phys. Rev. Lett.* **116**, 066804 (2016).
59. Baker-Jarvis, J., Vanzura, E. J. & Kissick, W. A. Improved technique for determining complex permittivity with the transmission/reflection method. *IEEE Transactions Microw. Theory* **38**, 1096–1103 (1990).
60. Luukkonen, O., Maslovski, S. I. & Tretyakov, S. A. A stepwise Nicolson-Ross-Weir-based material parameter extraction method. *IEEE Antennas Wirel. Propag. Lett.* **10**, 1295–1298 (2011).
61. Merano, M. Fresnel coefficients of a two-dimensional atomic crystal. *Phys. Rev. A* **93**, 013832 (2016).
62. Huidobro, P. A., Kraft, M., Maier, S. A. & Pendry, J. B. Graphene as a tunable anisotropic or isotropic plasmonic metasurface. *ACS Nano* **10**, 5499–5506 (2016).
63. Moroz, A. Exponentially convergent lattice sums. *Opt. Lett.* **26**, 1119–1121 (2001).
64. Lunnemann, P. & Koenderink, A. F. Dispersion of guided modes in two-dimensional split ring lattices. *Phys. Rev. B* **90**, 245416 (2014).
65. Belov, P. A. & Simovski, C. R. Homogenization of electromagnetic crystals formed by uniaxial resonant scatterers. *Phys. Rev. E* **72**, 026615 (2005).

66. Poddubny, A. N., Belov, P. A., Ginzburg, P., Zayats, A. V. & Kivshar, Y. S. Microscopic model of Purcell enhancement in hyperbolic metamaterials. *Phys. Rev. B* **86**, 035148 (2012).
67. Chebykin, A. V., Gorlach, M. A. & Belov, P. A. Spatial-dispersion-induced birefringence in metamaterials with cubic symmetry. *Phys. Rev. B* **92**, 045127 (2015).
68. Tretyakov, S. A., Viitanen, A. J., Maslovski, S. I. & Saarela, I. E. Impedance boundary conditions for regular dense arrays of dipole scatterers. *IEEE T. Antenn. Propag.* **51**, 2073–2078 (2003).
69. Silveirinha, M. G. & Fernandes, C. A. A new acceleration technique with exponential convergence rate to evaluate periodic Green functions. *IEEE Transactions Antenn. Propag.* **53**, 347–355 (2005).
70. Capolino, F., Wilton, D. R. & Johnson, W. A. Efficient computation of the 3D Green's function for the Helmholtz operator for a linear array of point sources using the Ewald method. *J. Comput. Phys.* **223**, 250–261 (2007).
71. Olmon, R. L. *et al.* Optical dielectric function of gold. *Phys. Rev. B* **86**, 235147 (2012).
72. Correas-Serrano, D., Gomez-Diaz, J., Tymchenko, M. & Alù, A. Nonlocal response of hyperbolic metasurfaces. *Opt. Express* **23**, 29434–29448 (2015).
73. Dmitriev, P. kitchenknif/pyatmm: V1.0.0-a1, https://doi.org/10.5281/zenodo.1041040 (2017).

## Acknowledgements

This work was partially supported by the Villum Fonden, Denmark through the DarkSILD project (No. 11116), Megagrant (No. 14.Y26.31.0015), the Ministry of Education and Science of the Russian Federation (3.1365.2017/4.6, 3.1668.2017/4.6, 3.8891.2017/8.9), RFBR (16-32-60123, 16-37-60064, 17-02-01234, 18-32-00739), the Grant of the President of the Russian Federation (MK-403.2018.2) and the Foundation for the Advancement of Theoretical Physics and Mathematics "BASIS" . The authors are thankful to M. Gorlach and A. Poddubny for the fruitful discussions and critical comments and to K. Ladutenko for the additional simulations.

## Author Contributions

O.Y. and F.P. performed the theoretical calculations. O.Y., D.P. and P.D. performed the numerical calculations. R.M. fabricated the samples. D.P. and A.S. conducted the measurements. A.S., I.I., A.A. and A.L. supervised the project. The paper was written by O.Y., A.A. and A.L. All authors discussed the results and reviewed the manuscript.

## Additional Information

**Supplementary information** accompanies this paper at https://doi.org/10.1038/s41598-018-32479-y.

**Competing Interests:** The authors declare no competing interests.

**Publisher's note:** Springer Nature remains neutral with regard to jurisdictional claims in published maps and institutional affiliations.

**Open Access** This article is licensed under a Creative Commons Attribution 4.0 International License, which permits use, sharing, adaptation, distribution and reproduction in any medium or format, as long as you give appropriate credit to the original author(s) and the source, provide a link to the Creative Commons license, and indicate if changes were made. The images or other third party material in this article are included in the article's Creative Commons license, unless indicated otherwise in a credit line to the material. If material is not included in the article's Creative Commons license and your intended use is not permitted by statutory regulation or exceeds the permitted use, you will need to obtain permission directly from the copyright holder. To view a copy of this license, visit http://creativecommons.org/licenses/by/4.0/.

© The Author(s) 2018